B2 1144+35: A Giant Low Power Radio Galaxy with Superluminal Motion

G. Giovannini[1,2], G.B. Taylor[3], E. Arbizzani[2], M. Bondi[2], W.D. Cotton[4], L. Feretti[2], L. Lara[5] and T.Venturi[2]

==

Astrophysical Journal - in press

==

ABSTRACT

We report on centimeter VLA and VLBI observations of the giant, low power radio galaxy 1144+35. These observations are sensitive to structures on scales from less than 1 parsec to greater than 1 megaparsec. Diffuse steep spectrum lobes on the megaparsec scale are consistent with an age of $\sim 10^8$ years. On the parsec scale, a complex jet component is seen to move away from the center of activity with an apparent velocity 2.7 h_{50}^{-1} c. It shows a central spine – shear layer morphology. A faint parsec scale counterjet is detected and an intrinsic jet velocity of 0.95 c and angle to the line of sight of 25° are derived, consistent with an intrinsically symmetric ejection. The central spine in the parsec scale jet is expected to move at a higher velocity and a Lorentz factor $\gamma \sim 15$ has been estimated near the core. The age of this inner VLBI structure is ~ 300 years. Assuming a constant angle to the line-of-sight, the jet velocity is found to decrease from 0.95 c at 20 mas (32 pc on the plane of the sky) to 0.02 c at 15 arcsec (24 kpc on the plane of the sky). These findings lend credence to the claim that (1) even the jets of low power radio galaxies start out relativistic; and (2) these jets are decelerated to subrelativistic velocities by the time they reach kiloparsec scales.

Subject headings: radio continuum: galaxies — galaxies: individual (B1144+35) — galaxies: jets — galaxies: nuclei

[1]Dipartimento di Fisica, Universita' di Bologna,via B.Pichat 6/2, 40127 Bologna, Italy

[2]Istituto di Radioastronomia del CNR, via Gobetti 101, 40129 Bologna, Italy

[3]National Radio Astronomy Observatory, P.O. Box 0, Socorro NM 87801, USA

[4]National Radio Astronomy Observatory, 520 Edgemont Rd, Charlottesville VA 22903-2475, USA

[5]Instituto de Astrofisica de Andalucia, CSIC, Apdo 3004, 18080 Granada, Spain

1. Introduction

This paper presents new data on a low power radio galaxy (B2 1144+35) belonging to a complete sample of radio galaxies which we are studying with VLBI data (Giovannini et al. 1990). A major result from this study is the discovery that at least in many, and perhaps in all, low power FR I radio galaxies (see Fanaroff & Riley 1974) parsec scale jets move at relativistic velocities. The derived velocities and orientations with respect to the line of sight (see e.g. Lara et al. 1997 and references therein) support the low-power unified scheme (see e.g. Urry & Padovani 1995) and suggest that multi-epoch observations should reveal a proper motion in many FR I galaxies. Up to now such studies have been carried out only on a small number of low power radio galaxies (e.g. M87, Biretta & Junor 1995; 3C338, Giovannini et al. 1998a; NGC 315 Cotton et al. 1998), it is therefore important to examine a larger number of FR I radio galaxies with multi-epoch observations to measure jet proper motions.

The low power radio galaxy B2 1144+35 discussed here, has been identified with a faint (m_{pg} = 15.7) Zwicky galaxy (ZW186.48) in a medium-compact galaxy cluster at a redshift of 0.0630. An isocontour image taken from the Palomar Observatory Sky Survey (POSS) is shown in Fig. 1. The contour image shows that the optical galaxy has a boxy shape which, according to Binney & Petrou 1985, may occur in systems that have cannibalized low luminosity galaxies. A nearby faint companion is embedded in its external region but optical spectroscopy is necessary to confirm a genuine connection. In a recent optical study of bright flat spectrum radio sources, Marcha et al. 1996 classify 1144+35 as a BL Lac candidate even though its spectrum shows Hα and [NII] emission lines (Colla et al. 1975, Morganti et al. 1992). From a comparison between the measured line equivalent width and the contrast Marcha et al. 1996 suggest that 1144+35 could be a diluted BL Lac. Moreover it was observed in an imaging and spectroscopic survey of low and intermediate power radio galaxies (Ebneter 1989). A CCD residual image shows a very definite arc of dust in the galaxy nuclear region.

The radio galaxy 1144+35 was detected in the X-Ray ROSAT All-Sky Survey (Brinkman et al. 1995) with a flux of 7.1 $\times$ 10^{-13} erg cm^{-2} sec $^{-1}$ in the 0.1–2.4 Kev band. Schoenmakers et al. 1999 derived from HRI ROSAT observations an X-Ray flux density of 8.1 $\times$ 10^{-13} erg cm^{-2} sec $^{-1}$ using a powerlaw model and 6.1 $\times$ 10^{-13} erg cm^{-2} sec $^{-1}$ using a thermal bremsstrahlung model, in the 0.1–2.4 Kev band.

From the radio point of view, 1144+35 has a peculiar structure: Machalski 1998 classifies it among giant radio galaxies, yet from high resolution VLA observations (Fanti et al. 1987) it has been classified a *naked* jet source since it shows two faint jet-like regions and no extended emission. The radio structure is core dominated and the two jet-like features are short and resolved. Schoenmakers et al. 1999 observed this source with the Westerbork Synthesis Radio Telescope (WSRT) at 1.4 GHz and reported WSRT observations at 325 MHz from the WENSS survey (Rengelink et al. 1997). They present a detailed image of the radio core and of two diffuse extended radio structures on either side of it. The eastern extended lobe shows a leading hotspot and is clearly associated with the central source. The northern part of the western radio structure is a separate low power radio galaxy; the southern part is a radio lobe with an elongated tail most likely associated with 1144+35.

The first VLBI observations of this source were carried out by Giovannini et al. 1990 with the EVN + Haystack with 2 scans, 13 minutes each. The source was detected, but the short on source integration time and the poor u, v coverage did not allow a discussion of its structure. It was imaged as part of the Second Caltech-Jodrell survey (Henstock et al. 1995) at 5 GHz, where it shows two main knots with some substructure. A preliminary study of the data from 3 epochs suggested the presence of a possible superluminal motion (Giovannini et al. 1995).

The new VLA, MERLIN and VLBI data presented in this paper demonstrate a complex structure over a broad range of physical scales (1 pc – 1 Mpc) and confirm superluminal motion. We also discuss some possible explanations for the structure of this peculiar radio galaxy. We use an Hubble constant $H_0 = 50$ km sec^{-1} Mpc^{-1} which corresponds to a conversion factor of 1.62 pc/mas.

2. Observations and Data Reduction

2.1. VLA Data

On November 1997, we obtained 6 hours of observing time with the VLA of the NRAO[6] in the D configuration at 1.4 and 5 GHz to investigate the large scale structure of 1144+35. The data have been calibrated in the standard way using the NRAO AIPS package and imaged using the task IMAGR. Calibrated data at 1.4 GHz were combined with a short (20 minutes long) VLA observation at higher resolution (C array) obtained in September 1997, to have better angular resolution while 5 GHz data were combined with a long observation also in the C configuration obtained in November 20, 1990 during a VLBI run with the VLA used as a phased array. In this run the source was observed for 12 hours, with the array phased every 15 minutes with a nearby VLA calibrator source. Since the arcsecond radio core is variable (see Sect. 3.4), a fraction of its flux was subtracted from the November 1990 observations before of combining the two datasets. The angular resolution and sensitivity of the images presented in this paper are given in Table 1.

The arcsecond scale radio emission of this source was observed with the VLA in the A-array configuration at 1.4, 5 and 8.4 GHz, on April 1994 and February 1997. Moreover, on September 1997, 1144+35 was observed at 15, 22.5 and 43 GHz for the VLA calibrator list. The source was observed for about 10 minutes total at each frequency in a few different hour angles to obtain better u, v coverage. The core flux density was derived by fitting a gaussian to the nuclear source. In these images due to the lack of short spacings and the short integration time, only the unresolved arcsecond core is visible and therefore we will use these data only to discuss the arcsecond core variability in the next sections.

2.2. MERLIN Data

We observed 1144+35 with the MERLIN array on 1995 March 29 at 5 GHz with a 16 MHz bandwidth for 10 hours. We used the following telescopes: Defford, Cambridge, Knockin, Wardle, Darnhall, MK2 and Tabley. The data were edited and amplitude calibrated in Jodrell Bank (JB) using the standard procedure based on the OLAF programs. 3C286 was used as amplitude calibrator. The data where then written in FITS format and loaded into AIPS where the phase calibration was carried out using standard MERLIN phase calibrators. The pipeline available in Jodrell Bank was used as a first step for the phase corrections only. The source was then mapped in total continuum and polarization and then self-calibrated.

---

[6] The National Radio Astronomy Observatory is operated by Associated Universities, Inc., under cooperative agreement with the National Science Foundation

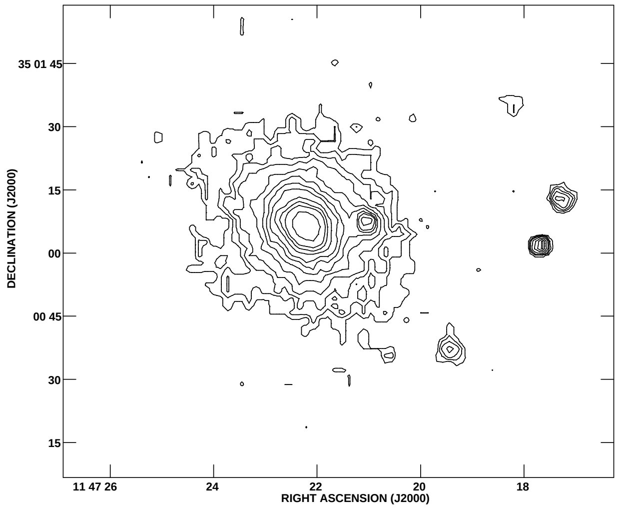

Fig. 1.— Optical image of 1144+35 from the Digitalized Palomar Sky Survey

Table 1: VLA image parameters

Array	Frequency GHz	HPBW ″	noise mJy/b	Figure N.	notes
C+D	1.4	20	0.06	2	I map
C+D	4.9	20	0.015	3	I map
C+D	4.9	20	0.012	3	P map
C+D	4.9	11	0.014	4	I map
C	4.9	3.5	0.06	6	I map

Note. — See Figure captions for more details; I map is the total intensity image; P map is the Polarized image used to draw E-vectors superimposed to the total intensity images.

2.3. VLBI Data

In Table 2 we summarize the VLBI observations which are discussed in the present paper. Data marked 1, 2 and 4 are discussed here for the first time, while the other are *literature* data.

The data have been correlated with the Caltech/JPL Block 2 correlator in Pasadena (Mk2 VLBI data) and in Socorro with the NRAO VLBA correlator (VLBA and global VLBI data). Amplitude calibration was then done using the standard system temperature method in AIPS. Data were globally fringe fitted and self-calibrated in the standard way. We made some iterations of phase self-calibration, followed by a final phase and gain self-calibration when necessary to produce the final image. Cross-hand correlations were produced for the September 1997 global 8.3 GHz observations only. Calibration of the instrumental leakage terms was performed using 4 widely spaced scans on the compact, unpolarized source OQ208 (Roberts et al. 1994). The absolute electric vector position angles were calibrated using two 5 minute scans on 3C279 which has a long-lived jet component of constant polarization angle (Taylor 1998).

Multi-frequency and snap-shot (see note to Table 2) observations were carried out switching often between frequencies or among different sources to obtain good and uniform u, v coverage. All other observations are long integration observations typically of 8 – 10 hours each. Mk2 data have been obtained with the old Mark2 system with a 2 MHz bandwidth and in single polarization mode; VLBA observations are in single polarization mode with 32 MHz bandwidth, while the global observation is a dual polarization, 64 MHz bandwidth observation. In this latest global observation, we used the following array for the total intensity images: Effelsberg, Noto, VLBA, and a single VLA antenna. Noto was not used for polarization images.

3. Results

3.1. The Megaparsec Scale

In agreement with Schoenmakers et al. 1999, we distinguish 3 different regions in the large scale structure of 1144+35: the core region, the East, and the West extended emission (see Figs. 2,3 and 4). The core region coincides with the optical galaxy and is the dominant feature in all the images. The core properties will be discussed in detail in Sect. 3.4.

The East extended emission shows an S shaped morphology and an uniform low brightness. It is clearly connected to the arcsecond core emission even if there is a strong discontinuity in the brightness of the inner nuclear region with respect to the extended lobe. Two small unresolved regions (see Fig. 4) are visible at the edge of the extended emission but are most likely unrelated background sources. The size of this extended emission is $\sim$6' (580 kpc).

The extended emission on the west side can be divided into two regions: north and south. The northern part is clearly an unrelated double radio galaxy (see Fig. 4) with a central core and two extended symmetric lobes. It is identified with a galaxy belonging to the same group as 1144+35 (Schoenmakers et al. 1999). To the south of this radio galaxy we find an extended emission which cannot be associated with the nearby field galaxy because of the strong asymmetry and the lack of any direct connection. It is opposite to the eastern emission of 1144+35 and we tentatively identify it as the west lobe of 1144+35. If 1144+35 is a giant double radio galaxy, it has an angular size of $\sim$ 13' corresponding to a projected linear size $\sim$ 1.3 Mpc and a total radio power at 1.4 GHz $\sim 1.24 \times 10^{25}$ W Hz^{-1}.

Table 2: History of VLBI Observations

Epoch mm-yy	Array 1.4GHz	Array 5.0GHz	Array 8.3GHz	Array 15.3GHz	Array 22.2GHz
11-90		Mk2[1]			
11-92	Mk2[1]				
06-93		Mk2[5]			
01-95				VLBA[3]	
03-95	VLBA[2]		VLBA[2]		
08-95		VLBA[4]			
11-95	VLBA[1]	VLBA[1]	VLBA[1]		
02-96					VLBA[3]
08-96		VLBA[4]			
09-97			GLOBAL[1]		

Note. — 1 – Full synthesis (8-10 hours long) observations; 2 – 5×6 min. snap-shots; 3 – see D. Henstock, 1996; 4 – 8×6 min. snap-shots with 8 MHz bandwidth; 5 – see Henstock et al. 1995.

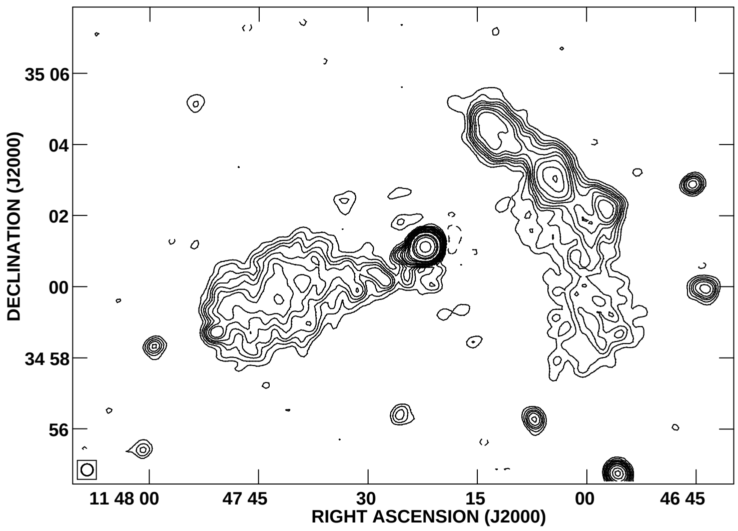

Fig. 2.— VLA image at 1.4 GHz. The HPBW is 20" and the noise level is 0.06 mJy/beam. The peak flux is 539.4 mJy/beam and contour levels are: -0.2 0.15 0.3 0.5 0.7 1 1.5 2 3 5 7 10 30 50 100 300 mJy/beam.

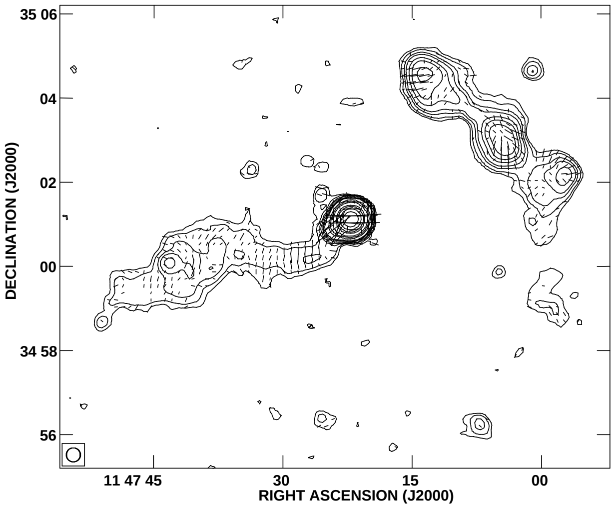

Fig. 3.— VLA image at 4.9 GHz. The HPBW is 20" and the noise level is 0.015 mJy/beam. Contour levels are: 0.05 0.1 0.2 0.3 0.5 0.7 1 3 5 10 30 50 100 200 mJy/beam. Lines are proportional to the polarized intensity and are oriented as the Electric field.

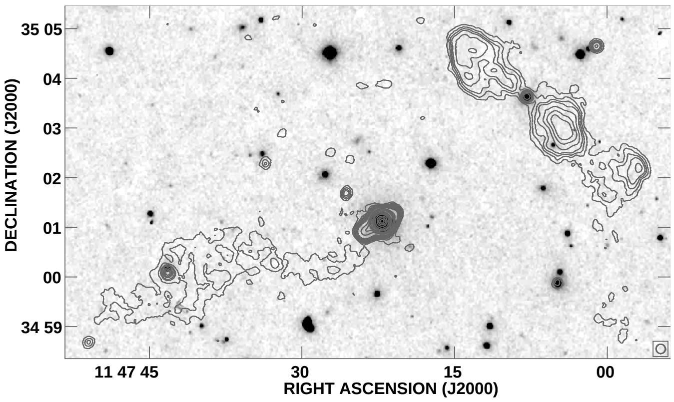

Fig. 4.— VLA image at 4.9 GHz superimposed on an optical image from the Digitized POSS. The HPBW is 11" and the noise level 0.014 mJy/beam. The peak flux is 442.28 mJy/beam and contour levels are: −0.08 0.05 0.1 0.15 0.2 0.3 0.4 0.5 0.7 1 2 4 6 8 10 30 50 100 200 300 400 mJy/beam.

To study the spectral index distribution of the extended emission, we made two images at 1.4 and 5 GHz with u, v coverage as similar as possible. To accomplish this we removed the short baselines in the 1.4 GHz data and the long baselines at 5 GHz and obtained two images with a HPBW = 30" to enhance the sensitivity of the 5 GHz image to low brightness features. After correcting for the primary beam attenuation we obtained a spectral index map between these two frequencies. In Fig. 5 we show the spectral index map with some contour levels from the 5 GHz image to show the source structure. The central region of 1144+35 has a flat spectrum ($\alpha \sim 0.1 - 0.2$ with $S_\nu \propto \nu^{-\alpha}$). The east extension is in general very steep; it shows a spectral index $\alpha \sim 0.8$ near the core that steepens continuously to the east, reaching $\alpha \sim$ 2–2.5 in the more external regions. Only in a small region at RA $\sim 11^h\ 47^m\ 41^s$ where a discrete unrelated source is present we find $\alpha \sim 0.9$. A Comparison of the present result with the spectral index map between 0.3 and 1.4 GHz discussed by Schoenmakers et al. 1999 shows that the low frequency spectrum is flatter than the high frequency one suggesting the presence of a steepening in the spectrum due to synchrotron losses in an old radio structure. Future observations, better matched in angular resolution and u, v coverage, are necessary to confirm this point. In the SW extended emission we find $\alpha \sim 0.9$ where a maximum of the brightness is visible and $\gtrsim$1.5 - 2.0 in the extended region. A more detailed analysis is not possible due to poor sensitivity of the 5 GHz image to the extended low brightness structure and because of the large primary beam attenuation.

We used the 1.4 GHz data and the standard formulae for synchrotron radiation to calculate the minimum energy density (u_{min}) and the equipartition magnetic field H_{eq}. We assumed a random magnetic field, equally stored energy in relativistic electrons and heavy particles, a filling factor = 1 and a lower and upper frequency cutoff of 10 MHz and 100 GHz respectively. With these assumptions we found $u_{min} \sim 8 \times 10^{-14}$ erg cm^{-3} for the Eastern lobe and $u_{min} \sim 7 \times 10^{-14}$ erg cm^{-3} for the Western lobe. The H_{eq} is ~ 1 μG in both lobes. From the derived spectral index of radiating electrons and the magnetic field present in the Eastern lobe we can estimate the lifetime of radiating electrons suffering both synchrotron and inverse Compton losses. According to the Jaffe-Perola model (Jaffe & Perola 1974) that assumes a redistribution of electron pitch angles we derive an age in the range 5 to 9 $\times 10^7$ yrs.

3.2. The Kiloparsec scale

We observed 1144+35 with the VLA in C configuration at 5 GHz as part of a VLBI experiment, obtaining a high quality map at an angular resolution of 3.5" (see Fig. 6). This image shows in detail the high brightness central structure visible in lower resolution images. We see a central emission slightly extended in the E-W direction (arcsecond core) coincident with the optical galaxy and faint jets emerging on both sides. We will call the SE jet the main jet since it is longer and has a higher surface brightness. Two faint and extended substructures are visible: J1 and J2, while in the shorter counterjet only one (CJ1) is visible at about the same core separation as J1. We measured the j/cj brightness ratio at 10" and 15" from the core and obtained values of 3.6 and 1.1 respectively.

To derive a spectral index map between 1.4 and 5 GHz we used the FIRST image (Becker et al. 1995) and an image with same resolution and gridding from our 5 GHz data. Even though the 1.4 GHz data were obtained from a snapshot, we do not expect missing flux at this frequency because of the small angular size of the source. The main jet has a relatively flat spectrum: the spectral index is 0.3 and 0.45 in J1 and J2 respectively and 0.2 in between. Also CJ1 has a spectral index $\sim$0.35. This result confirms the value derived on larger scales (Fig. 5) and the abrupt change in the spectral index distribution between this arcsecond scale structure and the extended structure. The arcsecond core spectral index will be discussed

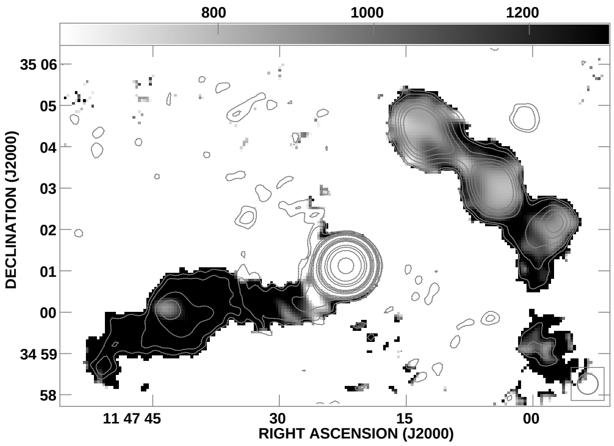

Fig. 5.— Spectral index map between 1.4 and 5 GHz. The grey scale is in milli-spectral index. Contour levels are from the 5 GHz image. The HPBW is 30".

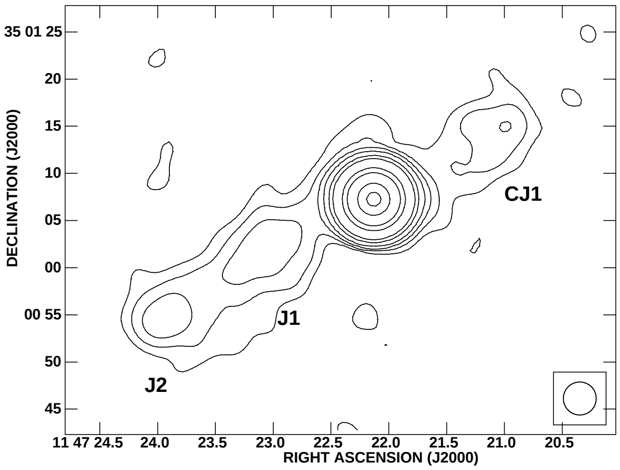

Fig. 6.— Total intensity image at 5 GHz; the HPBW is 3.5". Contour levels are: 0.2 0.5 1 2 5 10 50 100 300 mJy/beam. The noise level is 0.06 mJy/beam. Jet substructures are labelled according to Sect. 3.2.

in Sect. 3.4 because of the nuclear flux density variability.

3.3. Polarization Data on Kiloparsec to Megaparsec scales

The East lobe shows a high percentage polarized flux (at 1.4 GHz we find 15 to 30% in the more external lobe regions, $\sim$ 5% in the internal lobe region and up to 60% near the arcsecond nuclear region). At 5 GHz the polarization percentage has the same distribution with slightly higher values (from 30 to 70%). The polarization vectors at 1.4 and 5 GHz are oriented at about the same angle.

In the extended Western region associated with 1144+35, polarized flux is only detected in the brighter region. Here the polarization vectors are radially oriented and the fractional polarization is about 15 to 30% at 1.4 GHz. All the W radio emission does not show any change in the vector's angle between 1.4 and 5 GHz and its depolarization is low.

To better study the central region we obtained polarization images at 1.4 and 5 GHz with an HPBW of 11" (see Figs. 7,8). At this resolution the signal to noise ratio and the angular resolution allow us to separate the different components. At 5 GHz, in the core region, the electric field is oriented at 90° but at $\sim$ 15" from the core it changes to 0°, and then rotates again to gradually become aligned with the jet direction at $\sim$ 30" – 40" from the core. The 1.4 GHz vectors are rotated by $\sim$ 90° in the core, and the region 15" from the core is unpolarized. At 30" from the core the 1.4 GHz electric vectors are aligned with the 5 GHz vectors. In the counterjet we see a faint polarized emission oriented at $\sim$ 0° at 5 GHz and at $\sim$ 50° at 1.4 GHz.

The polarization percentage at 5 GHz is $\sim$ 20% at 30" from the core and decreases slowly to a few percent in the core. At 1.4 GHz we have a comparable percentage except in the region at 15" which is completely unpolarized at 1.4 GHz.

3.4. The arcsecond core

The arcsecond core of 1144+35 is the dominant feature of the radio emission from this galaxy and has long been known to be variable (Ekers et al. 1983). Its J2000 position is RA: 11^h 47^m 22.131^s DEC +35° 01' 07.52" (see Johnston et al. 1995 for a more accurate position). In Table 3 we report the arcsecond core flux densities available in the literature and the new results obtained by us, in order to study the flux variability and spectrum. Only core flux densities from high resolution data have been used so as to avoid contamination by the extended emission. The arcsecond core flux density is well sampled at 1.4 GHz from 1982 to 1998 and at 5 GHz from 1974 to 1998 while only sparse data at 8.4 and 15 GHz are available from 1990 onwards. We obtained one observation at very high frequencies (22 and 43 GHz) to study the high frequency spectrum (see Figures 9 and 14).

At 1.4 and 5 GHz we see an increase in the core flux density from 1974 to 1992 (1.4 GHz), and to 1994 (5 GHz). In this time range the core flux density increased by about a factor of 2. After 1980 the flux density variations are smooth on time scales less than a few years. Starting in $\sim$ 1990-1992 the core flux density decreases and we observe a delay in the decrease at lower frequencies possibly due to opacity effects.

We can derive the core spectral index by comparing observations at the same time or very near in time. Using 1997 data we have $\alpha \sim 0.43$ between 5 and 15 GHz and 0.30 between 15 and 43 GHz with a

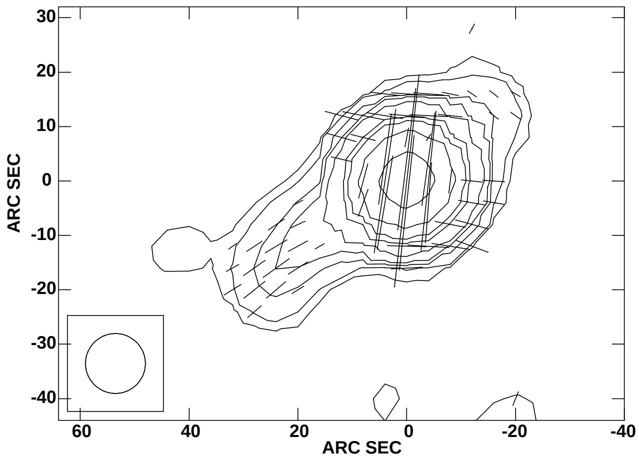

Fig. 7.— Total intensity image at 1.4 GHz with E field polarization vectors superimposed proportional to the polarized flux density; the HPBW is 11". Contour levels are: 0.5 1 3 5 10 30 50 100 300 mJy/beam.

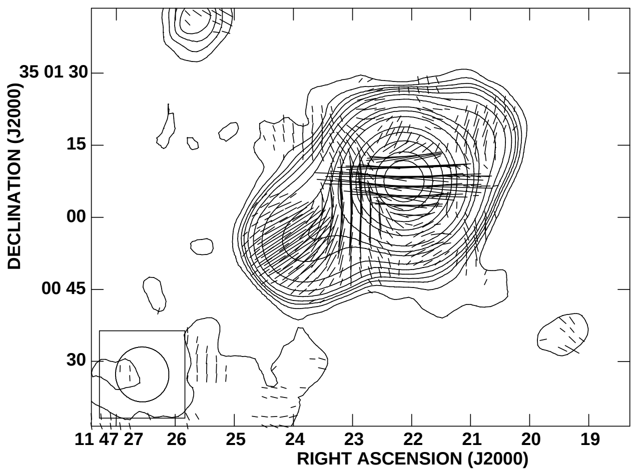

Fig. 8.— Total intensity image at 5 GHz with E field polarization vectors superimposed to the polarized flux density; the HPBW is 11". Contour levels are: 0.05 0.1 0.15 0.2 0.3 0.5 1 3 5 10 30 50 100 200 300 mJy/beam.

possible flattening between 1.4 and 5 GHz ($\alpha \sim$0.13, see Fig. 14). Data in the range 1.4 to 8.3 GHz are at the same epoch while data in the range 15 to 43 GHz were obtained 6 months apart. However, the slow variability and the suggestion of a constant spectral index in time indicates that this short delay should not influence the radio spectrum. The present results, obtained with almost simultaneous observations rule out the classification of the arcsecond core as a Gigahertz Peaked Spectrum (GPS) source suggested by Snellen et al. 1995 and Schoenmakers et al. 1999. Their conclusion was based on observations taken at too different epochs given the core flux density variability.

3.5. The parsec scale

3.5.1. Total intensity and spectral indices

In Figure 10 we present the full resolution image obtained with the MERLIN array at 5 GHz. It shows a central source with an extended emission ($\sim$ 100 mas) in the direction of the main jet and a marginally visible extension also in the opposite direction.

With the VLBA at 1.6 GHz the central source is resolved in a double structure (Fig. 11) with a weak emission at about 60 mas from the stronger component, in agreement with the MERLIN image at 5 GHz.

At 5 GHz with the VLBA, the parsec scale structure is resolved in four main substructures: two compact components (A and B in Fig. 12) separated by 3–4 mas, a discrete component (C) with a short symmetric extension located at about 20 mas from component A and a faint extended emission surrounding A and B components and clearly elongated in the direction of (C). The shape of this extended feature is not the same in the different epoch and frequency images due to different u, v coverage and sensitivity to low brightness structure, however the inner peak of this feature on the top (North) of A and B is always visible and we have named it A1 in Fig. 12.

In Figure 13 we show our most recent and highest resolution image at 8.4 GHz. The radio structure is very similar to the 5 GHz image, although C is clearly resolved into three components, labeled C, D and E. Component A1 is resolved into a complex structure roughly aligned with components C, D and E and the kpc-scale jet. A fairly compact component B1 has emerged just west of component B. There is also a clear bridge between components A and B.

The core variability found at arcsecond resolution implies that a flux density variability must be associated with some or all components detected in the parsec scale. We have compared the flux density taken at different epochs of components A, B, and C at the same frequency: component C is almost constant at 5 and 1.4 GHz while at 8.4 GHz it may have increased its flux density (58 mJy on March 1995; 65 mJy on September 1997). Components A and B follow the trend of the arcsecond core: their flux density slightly increases or is constant from 1990-94 and decreases in more recent observations. Since the flux density of component A ($\sim$ 185 mJy in the last 8.4 GHz map) is much higher than the B (30 mJy) and C (65 mJy) flux density it is clear that most of the arcsecond core flux density variability can be attributed to variability of component A.

To derive the spectral index of the different components we used the VLBA observation obtained on Nov. 26th, 1995 where the source was observed simultaneously at 1.4, 5, and 8.4 GHz. Moreover we used the flux densities at 15 and 22 GHz (Henstock 1996) which were not too far in time given that the flux density variability is a smooth function of time (see Section 3.4). The spectrum of components A, B, and C is shown in Figure 14 where we give also the arcsecond core spectrum at epoch 1997 for a comparison. We

Table 3: Arcsecond core flux densities

Epoch mm-yy	Flux(mJy) 1.4 GHz	Flux(mJy) 5.0 GHz	Flux(mJy) 8.3 GHz	Flux(mJy) 15 GHz	Flux(mJy) 22 GHz	Flux(mJy) 43 GHz	Ref.
01-73	340	-	-	-	-	-	1
01-74	-	290	-	-	-	-	1
12-74	-	310	-	-	-	-	2
02-75	-	310	-	-	-	-	2
04-75	-	330	-	-	-	-	2
12-75	-	340	-	-	-	-	2
08-76	-	395	-	-	-	-	2
01-77	-	425	-	-	-	-	2
02-80	-	500	-	-	-	-	2
08-82	529	-	-	-	-	-	3
12-84	568	-	-	-	-	-	4
05-85	568	-	-	-	-	-	5
02-90	-	-	501	-	-	-	6
11-90	-	551	-	-	-	-	pp
10-91	600	-	-	359	-	-	7
04-94	575	553	450	-	-	-	pp
08-94	-	537	-	-	-	-	8
07-95	570	-	-	-	-	-	8
02-97	569	483	393	-	-	-	pp
08-97	-	-	-	293	262	215	pp
08-97	541	-	-	-	-	-	9

Note. — References: 1) Colla et al. 1975; 2) Ekers et al. 1983; 3) Parma et al. 1986; 4) Fanti et al. 1986; 5) Fanti et al. 1987; 6) Patnaik et al. 1992; 7) Snellen et al. 1995; 8) Taylor et al. 1996; 9) Schoenmakers et al. 1999; pp) present paper.

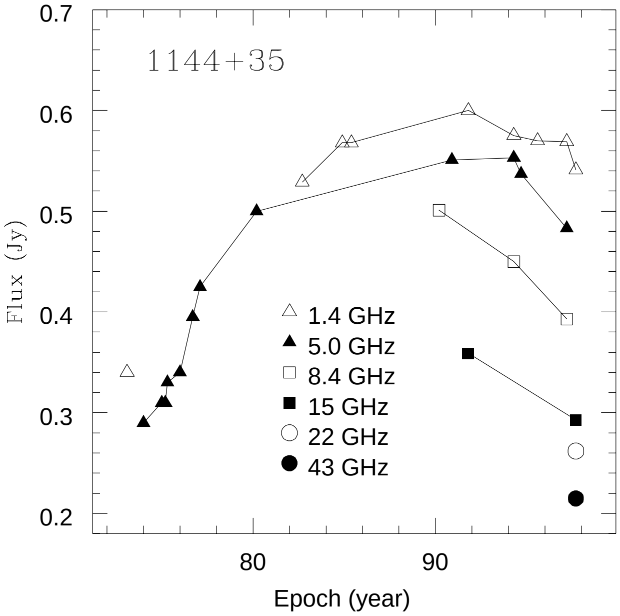

Fig. 9.— Arcsecond core flux densities at different epochs.

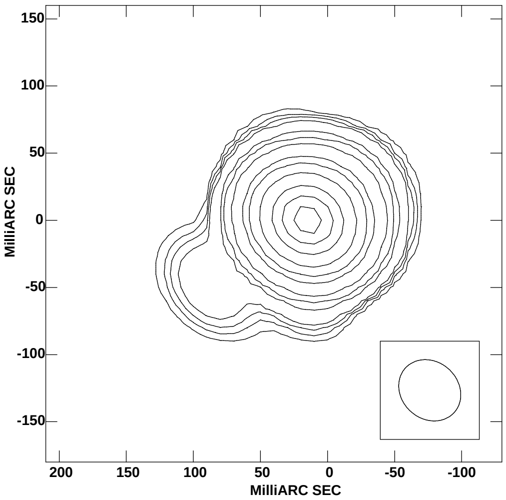

Fig. 10.— Full resolution MERLIN image of 1144+35 at 5 GHz. The HPBW is 49 × 42 mas in PA 50°. The noise level is 0.05 mJy/beam. Contour levels are: −0.3 0.3 0.5 0.7 1 3 5 10 30 50 100 200 300 400 mJy/beam.

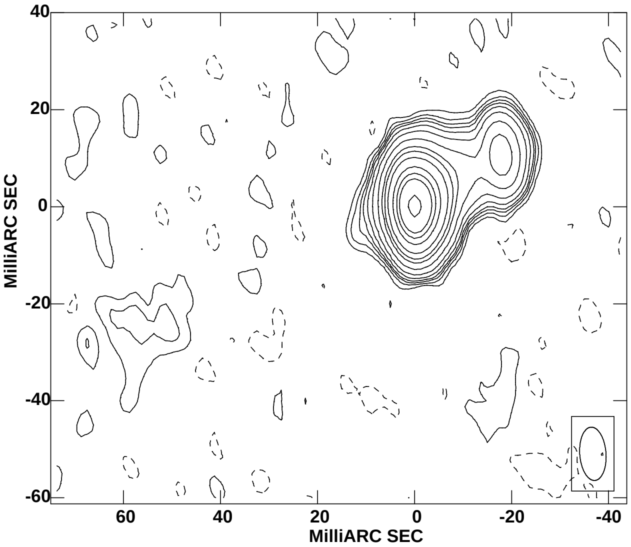

Fig. 11.— VLBA image at 1.4 GHz of 1144+35. The HPBW is 11 × 5 mas in PA 4°. The noise level is 0.25 mJy/beam. Contour levels are: −0.5 0.5 1 1.5 2 3 5 10 20 30 50 100 150 200 350 mJy/beam.

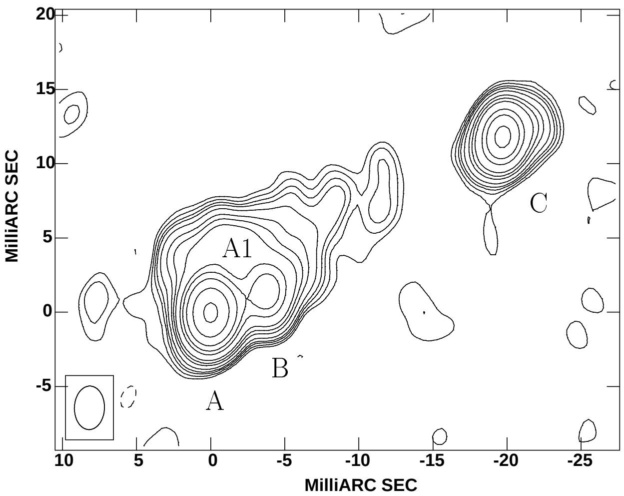

Fig. 12.— VLBA image at 5 GHz of 1144+35. The HPBW is 2.9 × 2.0 mas in PA -2°. The noise level is 0.4 mJy/beam. Contour levels are: −1 0.6 1 1.5 2 3 5 7 10 20 30 50 100 200 mJy/beam. Different components are labelled according to Sect. 3.5.1.

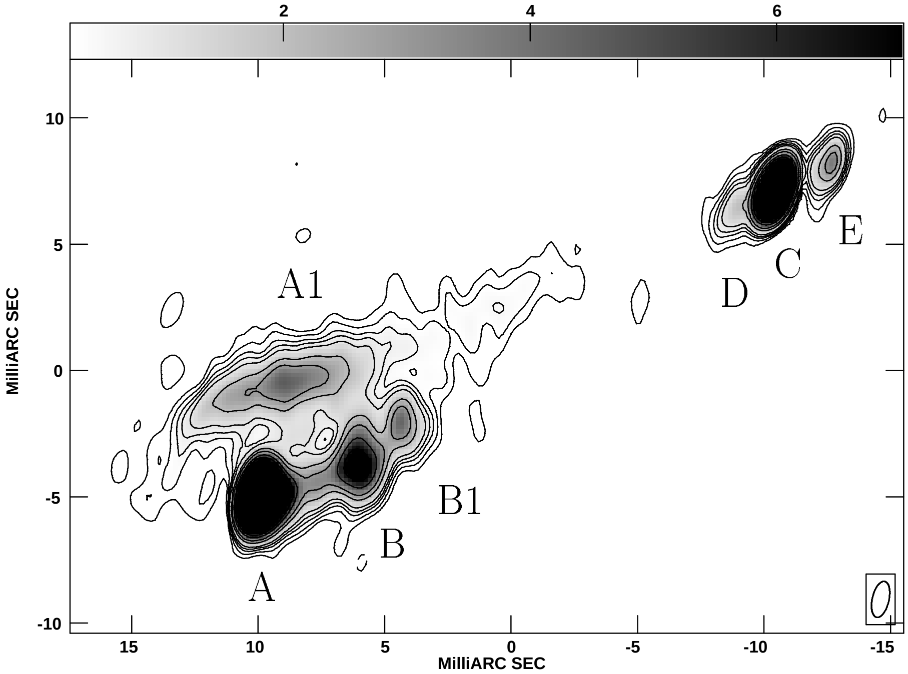

Fig. 13.— VLBI image at 8.4 GHz of 1144+35. The HPBW is 1.45 × 0.66 mas in PA −13°. The noise level is 0.05 mJy/beam. Contour levels are: −0.2 0.15 0.3 0.5 0.7 1 2 3 5 7 10 20 30 50 100 mJy/beam. Different components are labelled according to Sect. 3.5.1.

Table 4: Distances from the core at various epochs

Epoch dd/mm/yy	E mas	A mas	B mas	Frequency GHz
20/11/90	-	20.2	16.4	5.0
10/06/93	2.3	21.4	18.0	5.0
27/01/95	-	22.5	18.5	15
22/03/95	2.1	22.5	18.6	8.4
25/08/95	2.2	22.5	18.6	5.0
26/11/95	2.4	22.7	18.8	5.0
26/11/95	2.2	22.8	18.9	8.4
18/02/96	-	23.2	19.3	22
22/08/96	2.0	23.0	19.1	5.0
27/09/97	2.4	23.8	19.8	8.4

Note. — Positional uncertainties are ± 0.2 mas for the faint component E and ± 0.1 mas for A and B components (± 0.07 mas at 15 and 22 GHz).

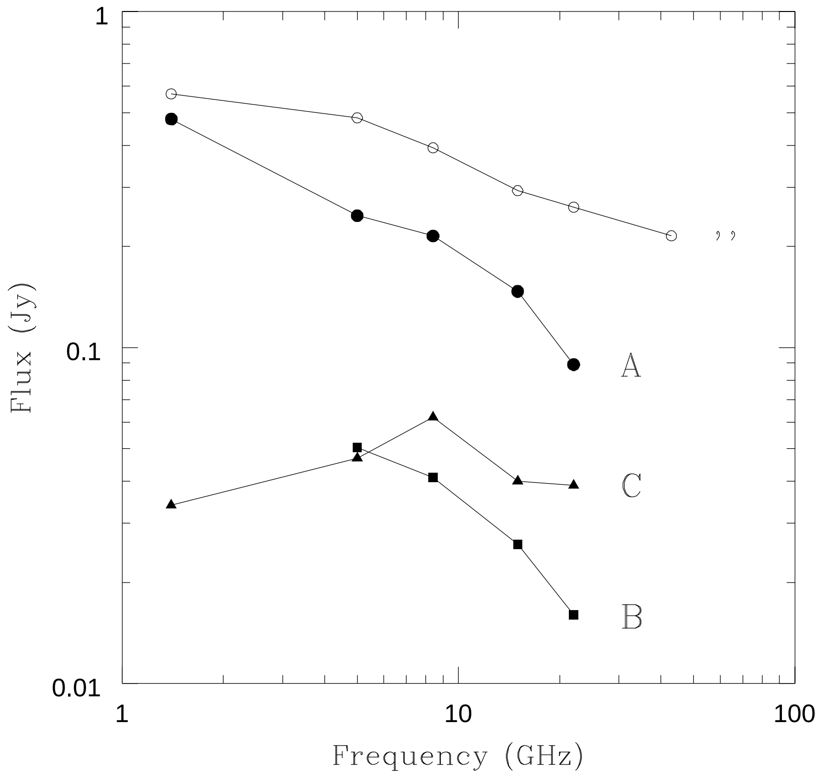

Fig. 14.— Radio spectrum of the arcsecond core (“ - open circles) from VLA data, 1997 epoch and of the components A, B and C (VLBI Nov. 26th, 1995 epoch).

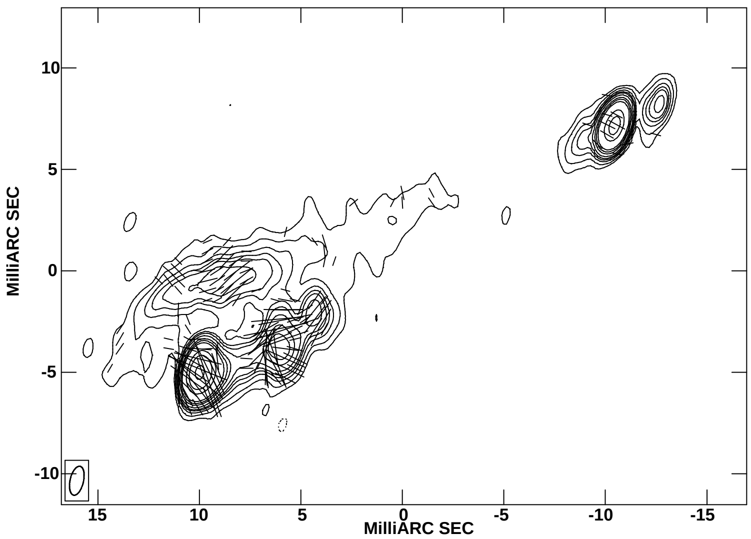

Fig. 15.— Same as Fig. 13, with E field polarization vectors superimposed proportional to the polarized flux density. Contour levels are: -0.2 0.2 0.5 1 1.5 2 3 5 7 10 30 50 100 mJy/beam.

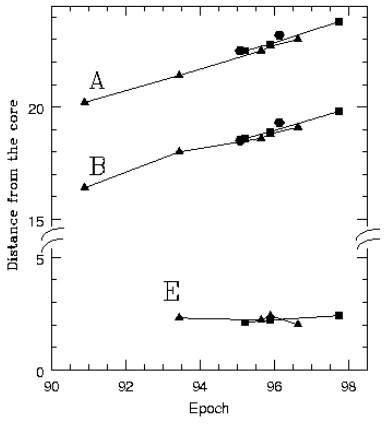

Fig. 16.— Core distance versus time of the A, B and E components. Triangles refer to 5GHz data, squares to 8.4 GHz data and hexagons to 15 and 22 GHz data. Positional uncertainties are not drawn for clarity; they are: $\pm$ 0.2 mas for component E and $\pm$ 0.1 mas for A and B components ($\pm$ 0.07 for 15 and 22 GHz data). Note that the *y axis* is not continuous.

do not show the spectrum of A1 since the flux density of this extended feature is strongly influenced by the different u, v coverages of the observations.

Components A and B show similar spectra: we derive for component A $\alpha_{8.4}^{1.4} = 0.45$ and $\alpha_{22.0}^{8.4} = 0.92$ while component B has $\alpha_{8.4}^{5.0} = 0.38$ and $\alpha_{22.0}^{8.4} = 0.98$. Component C has an inverted spectrum peaked around 8.4 GHz; $\alpha_{8.4}^{1.4} = -0.34$ and $\alpha_{22.0}^{8.4} = 0.45$ (see Fig. 14).

Based on its spectral properties we identify component C as the center of activity and the other components as parts of a parsec scale jet. The core is therefore self-absorbed with the maximum flux density at $\sim$ 8.4 GHz which implies a magnetic field of 3–5 Gauss. The two extended symmetric regions (D,E) visible at high resolution on both sides of the core component C are the base of a two sided symmetric jet structure. No further jet emission is visible on the NW side (counter jet side), while on the SE side (the jet side) we have the extended structure A, B, A1 and B1. Such a jet asymmetry will be discussed in Sect. 4.

We identify the extended complex structure A,A1,B,B1 as a clear evidence of a limb brightened jet: the maximum surface brightness is on the sides of a resolved jet. The projected jet opening angle is of $\sim$ 10°. Such a structure is expected by the *central spine - shear layer* jet model (Laing 1996). The image in Fig. 13 shows a gap of emission beyond D implying that the shear layer is not visible at the beginning but appears at $\sim$ 15 mas from the core. In this context we interpret the A, B and B1 structures as due to interaction of the parsec scale jets with an inhomogeneous surrounding medium (clouds?).

The alternative possibility that A1, D and E components are the parsec scale jet, as suggested by their alignment with the core, while A, B and B1 are shocked components ejected at a difference position angle with respect to the jet direction, appears more problematic. The good alignment of components A1, D and E with the core shows that this should be the present jet position angle and therefore A, B and B1 should be an older emission. However we note that A1 component looks more extended than A and B components, moreover the estimated velocity of A1 (see Sect. 3.5.3), even if affected by a large uncertainty, is very similar to the A and B measured velocity. Therefore we interpret the complex parsec scale morphology as a limb brightened jet with a relevant asymmetry on one side probably due to a strong interaction with a non symmetric external medium.

3.5.2. Polarization on the parsec scale

In Fig. 15 we present the total intensity VLBI image obtained from the Sept. 97 epoch observation at 8.4 GHz with polarized intensity vectors. Components A and B are polarized at the $\sim$ 0.4% and 1.2% level respectively, while the extended northern structure (A1) is polarized at a level of $\sim$ 5%. A fractional polarization of 0.3% (170 $\pm$ 30 μJy) was found at the core (C) position. The polarization angles are not aligned along any preferred orientation. This could indicate a disorder in the magnetic field and/or a high and changing Rotation Measure, either one of which is consistent with the low fractional polarization observed. This result is in agreement with the presence of a dense interstellar medium in the parsec scale region.

3.5.3. Proper Motion

We used the observations made at different epochs to measure the apparent proper motion of components A, A1, B, D, and E with respect to the core component C. First of all we compared observations obtained at the same frequency at different epochs to avoid any possible spurious result due to different spectral indices of components and afterwards we compared the results obtained using all the data. As expected from the uniform spectral index and the small size of components we found that the proper motion is only marginally related to the observing frequency and therefore we used all the data, except the 1.4 GHz ones where the angular resolution is too low to properly separate different components. In Table 4 and Fig. 16 we show the distance of components A, B, and E from C at each epoch. From these data we derive that no proper motion is measurable within the errors for component E ($\beta \lesssim 0.2$). Components A and B show a clear motion from the core C in the direction of the kiloparsec scale structure with a constant velocity. The average velocity is 2.78 ± 0.1 c for component A and 2.62 ± 0.1 c for component B. The motion of component A1 is not well determined because of the extended size and low surface brightness of this component. Comparing different epoch data we note that the radio emission centroid of A1 is always in between A and B components suggesting a similar velocity of A1 with respect to A and B. For component D no reliable measures were possible because of the lack of any visible substructure.

4. Jet Orientation and Velocity

From the measured apparent proper motion of the parsec scale jet, $\beta_a \sim 2.7\ \mathrm{h}_{50}^{-1}$, we can constrain the jet orientation (θ) and velocity (βc):

$$\beta = \beta_a/(\beta_a cos\theta + sin\theta)$$

We find that the 1144+35 jet has to move at a minimum intrinsic velocity of ∼ 0.94 c and that θ has to be smaller than 40°. The angle θ corresponding to the minimum velocity is ∼ 20°.

Assuming an intrinsic symmetry in the parsec scale structure of 1144+35, we identify the component E as the counterpart of the brightest region of the main jet, on the counter jet side. Due to the expected small viewing angle of the source with respect to the line of sight (see above), the size of the counterjet emission is expected to appear smaller than that of the jet emission. Therefore assuming intrinsic symmetry we can use the observational parameters to derive constraints on the velocity and orientation of this parsec scale jet independently of the Hubble constant as following:

1) Comparing the apparent velocity of the jet β_{aj}, and of the counterjet β_{acj}, we have (see e.g. Mirabel & Rodriguez 1994):

$$(\beta_{\mathrm{aj}} - \beta_{\mathrm{acj}})/(\beta_{\mathrm{aj}} + \beta_{\mathrm{acj}}) = \beta cos\theta$$

Given our limit on $\beta_{\mathrm{acj}} \lesssim 0.2$, we find:

$$\beta cos\theta \gtrsim 0.86.$$

2) From the jet – counterjet arm ratio (Giovannini et al. 1998a, Taylor & Vermeulen 1997), we derive:

$$\beta cos\theta \sim 0.82.$$

Comparing different constraints, we conclude that the 1144+35 jet has an intrinsic high velocity ∼ 0.95c or higher at a small angle with respect to the line of sight (25° or smaller). Given the large size of the extended emission and assuming no large difference in the orientation from the parsec to the Megaparsec scale structure, we will assume a value of $\theta \sim 25°$. With this orientation with respect to the line of sight and with $\beta \sim 0.95$, the Doppler factor δ is ∼ 2.25, the intrinsic jet opening angle is ∼ 4.2° and the total linear size of the source becomes ∼ 3 Mpc putting it among the largest of giant radio galaxies.

An independent constraint on δ can be derived from the synchrotron-self-Compton (SSC) model of X-ray emission from the nuclear region (see Marscher 1987, Ghisellini et al. 1993). In principle when the core angular size and the non-thermal nuclear X-ray emission is known, the comparison between the predicted and observed X-ray flux density gives constraints on the Doppler factor. From the upper limit to the core size from our VLBI data ($\lesssim$flux density measured by Brinkman et al. 1995 is non-thermal nuclear emission, we derive a lower limit for δ (see also Giovannini et al. 1994). Taking 8.4 GHz as the core self-absorption frequency we find a Doppler factor δ larger than 1.4 in agreement with our previous estimate.

From the estimated intrinsic velocity of the parsec scale jet, we can derive that the A+B+A1+B1 complex was ejected from the central engine about 300 years ago in the source reference frame. In this context the D feature is a more recent ejection from the core whose proper motion is not yet visible due to the lack of visible sub-structures. We would predict that in the near future it should be possible to see this component moving away from the core. The velocity obtained above refers to the brightest jet region (the shear layer). The presence of a central jet region (spine) with a lower brightness can be due to a higher velocity of the inner jet region with respect to the brighter external jet regions. A higher velocity implies in our case a low Doppler factor and therefore the jet central spine moving at high velocity will be less visible than the external shear layer. Also the presence of a gap of emission between D and the extended jet emission could be due to a low Doppler factor of a fast moving jet. For the A and B structures (but A1 and B1 are very likely moving at the same velocity) we have derived a doppler factor $\delta \sim 2.25$. This value implies that the intrinsic radio emission is amplified of a factor 7.5 – 8. To justify the dimming in the surface brightness in the central region of the jet and the gap, we have to assume that the fast jet spine should move with a Lorentz factor $\gamma \sim 15$. A value of $\gamma \sim 15$ corresponds to a velocity ~ 0.998 c and a Doppler factor $\delta \sim 0.698$ which implies that the intrinsic radio emission is dimmed by a factor $\sim$ 0.4. This model assumes an intrinsically symmetric jet while our images show a clear difference between components A, B, B1 and A1. As discussed in Sect. 3.5.1 we assume that these inhomogeneities are due to the interaction of the external jet regions with an inhomogeneous and clumpy surrounding medium. If this is the case, the inner jet spine should not be affected by the interaction with the external medium.

A free expanding jet is expected to show an intrinsic opening angle $\sim 1/\gamma$, (see e.g. Salvati et al. 1998) while a well confined and collimated jet will show a smaller opening angle. For the present source the estimated value of $\gamma \sim 15$ ($1/\gamma \sim 4°$) is in very good agreement with the intrinsic jet opening angle derived before (4.2° if $\theta \sim 25°$).

In this scenario, at the jet beginning there is no or very little difference in velocity between the spine and the shear layer therefore the whole jet is doppler deboosted and we have a gap in the radio emission. At about 15 mas from the core (corresponding to a de-projected distance of $\sim$ 55 pc) the external jet regions are moving at a lower velocity because of their interaction with the surrounding medium and the shear layer becomes more visible being Doppler boosted, while the inner jet region is still moving at high velocity and consequently is de-boosted. The presence of component D near the core could have two possible explanations: (1) the jet is accelerating as found in NGC 315 (Cotton et al. 1998); or (2) the intrinsic brightness of the jet near the core is high and therefore component D is visible despite the dimming due to the de-boosting effect.

With the existing data we cannot exclude that a transversal asymmetry causes: (1) the difference between the A, B, B1 and A1 regions; (2) the low brightness in the jet central region; and (3) the gap near the core. Future multi-frequency observations of the polarized emission in the jet should help to clarify the degree of interaction between the jet and the surrounding medium. Furthermore, long term monitoring of the source should allow the detection of a proper motion in the counterjet side (component E). This measurement is important since it will constrain the intrinsic jet velocity and allow for a direct distance determination.

We found a similar parsec scale morphology with space VLBI observations of the BL-Lac object Mkn 501 (Giovannini et al. 1998b): in this source we see a centrally peaked jet moving at a velocity in the range 0.990 – 0.999c in the inner 40 – 45 pc from the core, which becomes limb brightened at a de-projected distance of $\sim$ 45 pc. This result reinforces the scenario of a jet which appears limb-brightened at some distance from the core ($\sim$ 40 – 50 pc) due to the brightness of the shear layer which has slowed down with respect to the central spine because of the interaction with the surrounding medium.

Assuming a constant value for θ, from the j/cj ratio on the kiloparsec scale we find a jet velocity of $\sim$ 0.28 c at 10" from the core and of 0.02 c at 15" from the core in agreement with the expected jet velocity decrease in low power radio galaxies (see e.g. 3C449, Feretti et al. 1999). Such a velocity cannot explain the armlength asymmetry visible at arcsecond resolution (see Fig. 6); we suggest in agreement with Schoenmakers et al. 1999 that the arcsecond arm ratio asymmetry is due to the interaction with an inhomogeneous external medium which is responsible also for the asymmetric Megaparsec structure of 1144+35.

5. Arcsecond Core Flux Density Variability

The arcsecond core flux density of 1144+35 increases from 1974 to $\sim$ 1994 and decreases from 1994 to 1998. As discussed before, the flux density variability is not due to the activity of the mas core but to changes in the A, B, A1, B1 complex, specially in the A component being the region with highest flux density on the parsec scale.

A model to explain such a flux density turn-over in GPS sources was presented by Snellen et al. 1998 and in agreement with Schoenmakers et al. 1999 it could explain the core flux density variability in the present source. In fact, according to the scenario discussed in Sect. 3.5.3 the flux density variation of a factor 2 between 1974 and 1994 can be related to a slowing down of the shear layer of the parsec scale jet which increases the Doppler factor and therefore the observed flux. To produce a factor 2 of increasing flux the Doppler factor had to be $\sim$ 1.7 taking into account that now it is estimated to be $\sim$ 2.25. Such a variation can be obtained if the velocity decreases from $\sim$ 0.98c to 0.95 c in the last $\sim$ 15 mas behind A.

The faster flux density increase from 1974 to 1980 followed by a slower increase from 1980 to 1994 (Fig. 9) implies a variable rate of the Doppler factor probably due to a velocity decrease not constant in time but with a stronger deceleration at the beginning.

The decreasing flux from 1995 to present days could be due to adiabatic losses if A (and B) are expanding. In an expanding component we expect a delay in the flux density decrease at lower frequencies due to opacity effects, as found in the 1144+35 core (see Fig. 9).

6. The Connection between the Large and Small Scale Structure

The large scale structure shows a clear discontinuity between the extended relaxed lobes and the high brightness arcsecond core and jets (Sect. 3.1). This discontinuity is confirmed by the spectral index map which shows a large change in the spectral index moving from the arcsecond jet to the extended East lobe. These observational data suggest two different phases in the life of this radio source: the extended structure is a relic emission with an age in the range 5 to 9 $\times$ 10^7 yrs as estimated in Sect. 3.1, while the emission on the arcsecond scale has a shorter dynamical age: assuming an average velocity of $\gtrsim$0.02 c for the arcsecond structure we derive an age of $\lesssim$1.0 $\times 10^7$ yr, taking into account projection effects. We note that the Megaparsec scale East lobe of this source shows similar physical properties and is very similar in shape to the extended relic source 1253+275, found at the periphery of the Coma cluster (Giovannini et al. 1991). We can speculate that if the core of 1144+35 had ceased its activity, the extended emission could no longer be recognized as due to the activity of the galaxy ZW186.48 but it would be considered a relic emission in a group of galaxies.

A merger event with a gas rich object as suggested also by the *boxy* shape of the optical image could be the origin of the restarted activity. The large number of *young* CSS or CSO sources showing evidence of a recent merger event (O'Dea 1998) confirms the correlation between these processes and the radio activity.

Moreover we note that the parsec scale jet emission does not decrease smoothly in our VLBI maps. The parsec scale jet appears to stop at $\sim$ 24 mas from the core even if we have some evidence from the MERLIN and the 20 cm VLBA map that a low level flux density emission is present at larger distance from the core, in the same position angle. This can be due to a dramatic expansion of the radio jet after the position of the A component with a correspondingly large decrease in the surface flux density, similar to the jet expansion visible in Mkn 421 and Mkn 501 (Giovannini et al. 1998b). Alternatively the A, A1, B, B1 complex could be a strong enhancement in the jet brightness due to a strong increase of the nuclear activity. This burst should have taken place about 300 yrs ago in the source reference frame, corresponding to $\sim$ 45 yrs in our reference frame. This hypothesis is in agreement with the core flux density variability discussed in the previous sections.

7. Conclusions

We present new VLA and VLBI observations of the low power radio galaxy 1144+35. These observations allow us to study and discuss the properties of this source from the Megaparsec to the parsec scale. 1144+35 is one of the few sources with observed two-sided parsec scale jets. These sources are of particular interest since they can be used to place constraints on the cosmological parameters H_0 and q_0. Moreover this source is oriented at $\sim$ 25° with respect to the line of sight therefore, in agreement with unified scheme models, presents properties in between FR I radio galaxies and BL-Lac type objects.

On the Megaparsec scale 1144+35 appears to be a giant radio galaxy: 1.3 Mpc on the plane of the sky corresponding to a deprojected linear size $\sim$ 3 Mpc. It shows an East lobe with an elongated shape, connected to the core emission and a Western extended emission interpreted as the West lobe of a double radio galaxy. The age of this emission is estimated to be 5 to 9 $\times$ 10^7 yrs.

At kiloparsec resolution, a core and a two-sided jet are present. The surface brightness and the spectral index distribution suggest a strong discontinuity between this structure and the Megaparsec scale emission. This observational result could be due to a change in the jet direction or to renewed activity in the galaxy core probably triggered by a galaxy merger.

The arcsecond core is the dominant feature of this source at arcsecond resolution. Its flux density showed a large increase from 1974 to 1980 (from 280 to 500 mJy at 5 GHz), followed by a smooth increase until 1992. From 1992 to date the core flux density has decreased; the flux density decrement appeared first at higher frequencies. The core spectrum obtained from same epoch observations is flat and we rule out the identification of the 1144+35 core as a GPS source.

At parsec resolution we identified the core source (C) and a two-sided jet emission very asymmetric in shape and properties. This asymmetry, when interpreted in the light of unified scheme models and of relativistic jets, constrains the jet velocity to be $\gtrsim$0.95c with an orientation with respect to the line of sight $\lesssim$25°. These results are in agreement with the detected proper motion with $\beta_a \sim 2.7$. The source orientation explains its properties intermediate between a FR I radio galaxy and a BL-Lac type object.

The parsec scale jet is limb brightened and its morphology is in agreement with the presence of a fast inner jet spine ($\beta \sim 0.998$) surrounded by a shear layer in which the velocity decreases because of the interaction with the surrounding medium. The estimated age of this structure is of $\sim$ 300 yrs in the source reference frame.

We thank R. Fanti, D. Dallacasa and G. Brunetti for critical reading of the manuscript and useful discussions. The Digitized Sky Survey was produced at the Space Telescope Science Institute under US Government grant NAG W-2166. This work was partly supported by the Italian Ministry for University and Research (MURST) under grant Cofin98-02-32

REFERENCES

Becker, R.H., White, R.L., Helfand, D.J. 1995 ApJ, 450, 559

Binney, J., Petrou, M. 1985, MNRAS, 214, 449

Biretta, J.A., Junor, W. 1995, Proc. Natl. Acad. Sci. USA, 92, 11364

Brinkman, W., Siebert, J., Reich, W., Fuerst, E., Reich, P., Voges, W., Truemper, J., Wielebinski, R. 1995 A&AS, 109, 147

Colla, G., Fanti, C., Fanti, R., Gioia, I., Lari, C., Lequeux, J., Lucas, R., Ulrich, M.H. 1975, A&AS, 20, 1

Condon, J.J., Cotton, W.D., Greisen, E.W., Yin, Q.F., Perley, R.A., Taylor G.B., Broderick, J.J. 1998, AJ, 115, 1693

Cotton, W.D., Giovannini, G., Feretti, L., Lara, L., Venturi, T. 1998, submitted to ApJ

Ebneter, K.A. 1989 Ph.D. Thesis California Univ. Berkeley

Ekers, R.D., Fanti, R., Miley, G.K. 1983, A&A, 120, 297

Fanaroff, B.L., & Riley, J.M. 1974, MNRAS, 167, 31

Fanti, C., Fanti, R., de Ruiter, H.R., Parma, P. 1986, A&AS, 65, 145

Fanti, C., Fanti, R., de Ruiter, H.R., Parma, P. 1987, A&AS, 69, 57

Feretti, L., Perley, R., Giovannini, G., Andernach, H. 1999 A&A, 341, 29

Ghisellini, G., Padovani, P., Celotti, A., Maraschi, L. 1993, ApJ, 407, 65

Giovannini, G., Feretti, L., Comoretto, G. 1990 ApJ, 358, 159

Giovannini, G., Feretti, L., Stanghellini, C. 1991, A&A, 252, 528

Giovannini, G., Feretti, L., Venturi, T, Lara, L., Marcaide, J., Rioja, M., Spangler, S.R., Wehrle, A.E. 1994, ApJ, 435, 116

Giovannini, G., Cotton, W.D., Feretti, L., Lara, L., Venturi, T, Marcaide, J. 1995, Proc. Natl. Acad. Sci. USA, 92, 11356

Giovannini, G., Cotton, W.D., Feretti, L., Lara, L., Venturi, T. 1998a, ApJ, 493, 632

Giovannini, G., Feretti, L., Venturi, T., Cotton, W.D., Lara, L. 1998b, to appear in the Proceedings of the "Bl Lac Phenomenon" Conf., held in Turku, 1998 - June 22,26 - ed. Leo Takalo (astro-ph/9810430)

Henstock, D.R., Browne, I.W.A., Wilkinson, P.N., Taylor, G.B., Vermeulen, R.,C., Pearson, T.J., Readhead, A.C.S. 1995, ApJS, 100, 1

Henstock, D.R. 1996, Ph.D. Thesis, University of Manchester

Jaffe, W.J., Perola, G.C. 1974, A&A, 31, 223

Johnston, K.J., Fey, A.L., Zacharias N. et al. 1995, AJ, 110, 880

Laing, R.A. 1996, A.S.P. Conf. Ser. 100, Hardee et al. eds, p. 241

Lara, L., Cotton, W.D., Feretti, L., Giovannini, G., Venturi, T., Marcaide, M. 1997, ApJ, 474, 179

Machalski, J. 1998, A&AS, 128, 153

Marcha, M.J.M., Browne, I.W.A., Impey, C.D., Smith, P.S. 1996, MNRAS, 281, 425

Marscher, A.P. 1987, in Superluminal Radio Sources, ed. J.A. Zensus and T.J. Pearson, Cambridge Univ. press, p. 280

Mirabel, I.F., Rodriguez, L.F. 1994, Nature, 371, 46

Morganti, R., Ulrich, M.-H., Tadhunter, C.N. 1992, MNRAS, 254, 546

O'Dea, C.P. 1998, PASP, 110, 493

Parma, P., de Ruiter, H.R., Fanti, C., Fanti, R. 1986, A&AS, 64, 135

Patnaik, A.R., Browne, I.W.A., Wilkinson, P.N., Wrobel, J.M. 1992, MNRAS, 254, 655

Rengelink, R., Tang, Y., de Bruyn, A.G., Miley, G.K., Bremer, M.N., Roettgering, H.J.A., Bremer, M.A.R. 1997, A&AS, 124, 259

Roberts, D.H., Wardle, J.F.C., Brown, L.F. 1994, ApJ, 427, 718

Salvati, M., Spada, M., Pacini, F. 1998, ApJ, 495, L19

Schoenmakers, A.P., de Bruyn, A.G., Roettgering, H.J.A., van der Laan, H. 1999 A&A, 341, 29

Snellen, I.A.G., Zhang, M., Schilizzi, R.T., Roettgering, H.J.A., de Bruyn, A.G., Miley, G.K. 1995, A&A, 300, 359

Snellen, I.A.G., Schilizzi, R.T., de Bruyn, A.G., Miley, G.K. 1998, A&A, 333, 70

Taylor, G.B., Vermeulen, R. C., Readhead, A.C.S., Pearson, T.J., Henstock, D.R., Wilkinson, P.N. 1996, ApJS, 107, 37

Taylor, G.B., & Vermeulen, R. C. 1997, ApJ, 485, L9

Taylor, G.B. 1998, ApJ, 506, 637

Urry, C.M., Padovani, P. 1995, PASP, 107, 803

This preprint was prepared with the AAS LaTeX macros v4.0.